Journal Name

PAPER # Response of a magnetically diverted tokamak plasma to a resonant magnetic perturbation

Richard Fitzpatrick⬥   Institute for Fusion Studies, Department of Physics, University of Texas at Austin, Austin

TX 78712, USA   **E-mail:** rfitzp@utexas.edu

Abstract
The safety-factor profile of a magnetically diverted tokamak plasma diverges logarithmically as the magnetic separatrix (a.k.a. the last closed magnetic flux-surface) is approached. At first sight, this suggests that, when determining the response of such a plasma to a static, externally generated, resonant magnetic perturbation (RMP), it is necessary to include an infinite number of rational magnetic flux-surfaces in the calculation, the majority of which lie very close to the separatrix. In fact, when finite plasma resistivity is taken into account, this turns out not to be the case. Instead, it is only necessary to include rational surfaces that lie in the region $0 < \Psi < \Psi_c$, where Ψ is the normalized poloidal magnetic flux, and $\Psi_c < 1$ can be calculated from the edge plasma parameters. It is estimated that $\Psi_c = 0.9985$ for an $n = 1$ RMP, and $\Psi_c = 0.9952$ for an $n = 4$ RMP, in a typical JET H-mode plasma.

1   Introduction

All modern tokamak plasmas feature a *magnetic divertor*, which is a particular configuration of the magnetic field that redirects the outermost field-lines away from the confined plasma region and into a controlled exhaust area where the plasma particle and heat fluxes can safely be absorbed by a solid target plate [1]. Each magnetic flux-surface in a tokamak plasma has an associated value of the *safety-factor*, which specifies the average number of toroidal circuits of the surface that a constituent magnetic field-line makes per poloidal circuit [2]. Magnetic flux-surfaces possessing rational values of the safety-factor are special. Indeed, externally generated, static, non-axisymmetric magnetic perturbations—known as *resonant magnetic perturbations* (RMPs)—can drive magnetic reconnection on such *rational surfaces*, leading to localized changes in magnetic topology that degrade the ability of the surrounding flux-surfaces to confine energy. Alternatively, shielding currents can flow, predominately parallel to magnetic field-lines, on rational surfaces, and act to suppress driven magnetic reconnection [3]. In general, neither driven magnetic reconnection nor shielding currents can occur on irrational magnetic flux-surfaces.

A magnetically diverted tokamak plasma possesses a so-called "last closed magnetic flux-surface" (LCFS). Magnetic flux-surfaces that lie inside the LCFS are topologically simple tori, and are completely occupied by plasma. Magnetic flux-surfaces that lie outside the LCFS have more complicated topology, and are only partialy occupied by plasma. The LCFS features a magnetic "X-point", which is a circular loop, coaxial with the plasma torus, on which the poloidal magnetic field is zero. (In some very special tokamak plasmas, the LCFS features two X-points. However, we shall not consider such plasmas here.) As the LCFS is approached, the safety-factor exhibits a logarithmic singularity [4], as a direct consequence of the presence of the X-point, and there is an associated accumulation of rational magnetic flux-surfaces in the vicinity of the LCFS. In fact, for an RMP with a given toroidal mode number, there are, in principle, an *infinite* number of associated rational surfaces, most of which lie very close to the LCFS, on which the RMP can drive magnetic reconnection. It is impossible to include all of these surfaces in a practical plasma response calculation. Hence, the standard approach is to simply ignore rational flux-surfaces associated with very high values of the safety-factor [5, 6, 7, 8, 9, 10, 11]. The purpose of this paper is to investigate to what extent this approach is justified.

This paper is organized as follows. A particularly simple model of a magnetically diverted tokamak plasma is introduced in Sect. 2, and is used to define exactly what is meant by a straight-field-line coordinate system, the safety-factor profile, and a rational surface, both inside and outside the LCFS. A more realistic model of a magnetically diverted tokamak plasma is presented in Sect. 3. The response of a magnetically diverted plasma to an RMP is analyzed in

Sect. 4. Section 5 investigates the behavior of the plasma response model in the vicinity of the LCFS. Finally, the paper is summarized in Sect. 6.

2   Simple model of a magnetically diverted plasma

2.1   Introduction

The aim of this section is to construct a very simple model of a magnetically diverted tokamak plasma.

2.2   Equilibrium magnetic field

Let x, y, z be conventional Cartesian coordinates. Suppose that two current filaments run parallel to the z-axis [4]. Let the first filament carry the current I_p, and pierce the x-y plane at $x = y = 0$. Let the second filament carry the current I_c, and pierce the x-y plane at $x = 0$, $y = -a$. The first filament represents the "toroidal" (i.e., z-directed) plasma current, whereas the second represents the toroidal current flowing in the magnetic divertor coil that generates the magnetic X-point. Suppose that there is a uniform, externally generated, toroidal magnetic field of strength B_0. Let the system be periodic in the z direction with period $2\pi R_0$, where R_0 is the simulated major radius of the plasma. It is helpful to define the simulated toroidal angle, $\phi = z/R_0$.

The equilibrium magnetic field can be written in the divergence-free manner

$$\mathbf{B} = \nabla\phi \times \nabla\psi_p + B_0 R_0 \nabla\phi, \tag{1}$$

where

$$\psi_p(x,y) = \frac{\mu_0 I_p R_0}{4\pi} \ln\left(x^2 + y^2\right) + \frac{\mu_0 I_c R_0}{4\pi} \ln\left[x^2 + (y+a)^2\right] \tag{2}$$

is the "poloidal" (i.e., circulating in the x-y plane) magnetic flux (divided by 2π) generated by the two current filaments.

2.3   Straight-field-line coordinates

It is convenient to re-express the magnetic field in the usual Clebsch form

$$\mathbf{B} = \nabla(\phi - q\,\theta) \times \nabla\psi_p, \tag{3}$$

where θ is a poloidal angle, and $q = q(\psi_p)$ the (dimensionless) *safety-factor* [12]. Equations (1) and (3) can be reconciled provided

$$\nabla\psi_p \times \nabla\theta \cdot \nabla\phi = \frac{B_0}{R_0 q}. \tag{4}$$

Note, from Eq. (3), that $\mathbf{B} \cdot \nabla\psi_p = 0$, which implies that ψ_p is a magnetic flux-surface label. Furthermore, $\mathbf{B} \cdot \nabla(\phi - q\,\theta) = 0$, which implies that magnetic field-lines within a given flux-surface appear as straight lines, with gradient $d\phi/d\theta = q$, when plotted in the θ-ϕ plane. In fact, ψ_p, θ, ϕ are known as *straight-field-line coordinates*, and θ is termed a *straight* poloidal angle [12]. The defining property of a straight-field-line coordinate system is the choice $q = q(\psi_p)$, rather than $q = q(\psi_p, \theta)$, or even $q = q(\psi_p, \theta, \phi)$. There are many types of straight-field-line coordinate systems (e.g., Hamada [13], Boozer [14], PEST [15], equal-arc), all of which have the required property that $q = q(\psi_p)$. For the sake of convenience, we have chosen to use PEST coordinates, which are characterized by a toroidal angle, ϕ, that corresponds to the polar angle in the R, ϕ, Z cylindrical coordinate system. (See Sect. 3.2.) Once the choice of toroidal angle is made, the coordinate system is uniquely defined.

2.4   Non-diverted edge safety-factor

In the absence of the divertor current, the plasma would have a circular cross-section of minor radius a, and an edge safety-factor value of

$$q_* = \frac{2\pi B_0 a^2}{\mu_0 I_p R_0}. \tag{5}$$

2.5   Normalization scheme

Let $x = a\,X$, $y = a\,Y$, $\nabla = a^{-1}\,\hat{\nabla}$, and $\psi_p = \mu_0 I_p R_0 \psi/(2\pi)$. It follows that

$$\hat{\nabla}\psi \times \hat{\nabla}\theta \cdot \nabla\phi = \frac{a}{R_0}\,\frac{q_*}{q}, \tag{6}$$

$$\psi(X,Y) = \frac{1}{2}\ln\left(X^2 + Y^2\right) + \frac{\zeta}{2}\ln\left[X^2 + (Y+1)^2\right], \tag{7}$$

$$\psi_X(X,Y) = \frac{X}{X^2 + Y^2} + \frac{\zeta\,X}{X^2 + (Y+1)^2}, \tag{8}$$

$$\psi_Y(X,Y) = \frac{Y}{X^2 + Y^2} + \frac{\zeta\,(Y+1)}{X^2 + (Y+1)^2}, \tag{9}$$

where $\zeta = I_c/I_p$. Here, $\psi_X \equiv \partial\psi/\partial X$, et cetera.

2.6   Magnetic X-point

The magnetic X-point is located at the point in the X-Y plane where $\psi_X = \psi_Y = 0$ (i.e., where the poloidal magnetic field-strength is zero). As is easily demonstrated, the coordinates of this point are (X_x, Y_x), where $X_x = 0$ and $Y_x = -1/(1+\zeta)$. The magnetic separatrix corresponds to the curve $\psi(X,Y) = \psi_x$, where

$$\psi_x \equiv \psi(X_x, Y_x) = \ln\left[\frac{\zeta^\zeta}{(1+\zeta)^{1+\zeta}}\right]. \tag{10}$$

It is helpful to define the normalized poloidal flux, $\Psi = \psi_x/\psi$. (Note that this definition is different from the conventional one, $\Psi = \psi/\psi_x$, because $\psi \to \infty$ on the magnetic axis, $X = Y = 0$, and we wish the normalized flux to increase as we go from the axis to the separatrix.)

2.7   Construction of straight-field-line coordinate system

Equation (6) yields

$$\frac{d\theta}{dL} = \frac{q_*}{q\,|\hat{\nabla}\psi|}. \tag{11}$$

where dL is an element of normalized length (in the X-Y plane) around a magnetic flux-surface. It follows that

$$q(\psi) = \frac{q_*}{2\pi}\oint\frac{dL}{|\hat{\nabla}\psi|}, \tag{12}$$

where $\oint$ implies a complete circuit in θ at constant ψ. It is easily demonstrated that, on such a circuit,

$$\frac{dX}{dL} = -\frac{\psi_Y}{\sqrt{\psi_X^2 + \psi_Y^2}}, \tag{13}$$

$$\frac{dY}{dL} = \frac{\psi_X}{\sqrt{\psi_X^2 + \psi_Y^2}}, \tag{14}$$

$$\frac{d\phi}{dL} = \frac{q_*}{\sqrt{\psi_X^2 + \psi_Y^2}}, \tag{15}$$

$$\frac{d\varpi}{dL} = \frac{X\,\psi_X + Y\,\psi_Y}{(X^2 + Y^2)\sqrt{\psi_X^2 + \psi_Y^2}}, \tag{16}$$

where

$$\varpi = \tan^{-1}\left(\frac{Y}{X}\right) \tag{17}$$

is a geometric poloidal angle. Here, ϕ is calculated on the assumption that we are following a magnetic field-line within the flux-surface (i.e., $d\phi/d\theta = q$). We need to integrate Eqs. (13)–(16) from $\varpi = 0$ to $\varpi = 2\pi$, subject to the initial condition $\phi(\varpi = 0) = 0$, and then set $q(\psi) = \phi(\varpi = 2\pi)/(2\pi)$. We can then compute θ using

$$\frac{d\theta}{dL} = \frac{q_*}{q\sqrt{\psi_X^2 + \psi_Y^2}}. \tag{18}$$

Let $q_* = 12$ and $\zeta = 0.2$. Figure 1 shows the magnetic flux-surfaces $\Psi = 0.9$, $\Psi = 1.0$, and $\Psi = 1.1$, plotted in the X-Y plane. Flux-surfaces characterized by $\Psi < 1$ do not enclose the divertor current filament, whereas those characterized by $\Psi > 1$ do enclose the filament. The *magnetic separatrix*, $\Psi = 1$, separates flux-surfaces that do and do not enclose the divertor current filament, and crosses itself at the magnetic X-point.
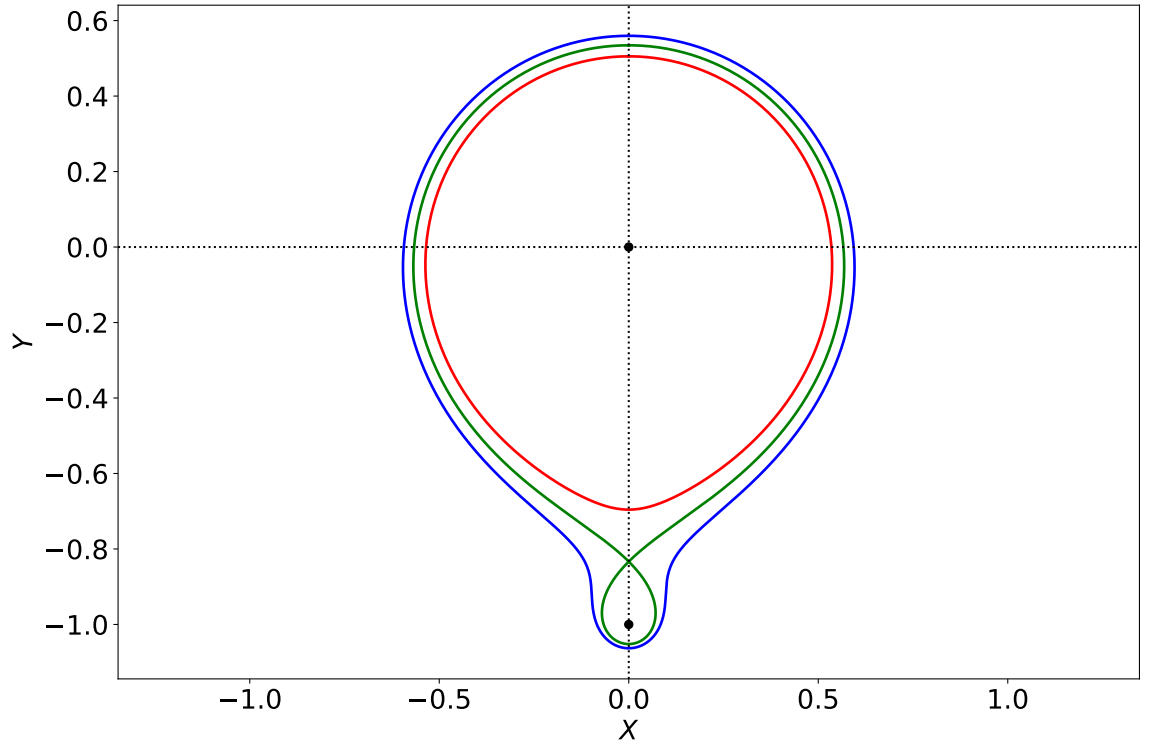
Figure 1. The magnetic flux-surfaces $\Psi = 0.9$ (red), $\Psi = 1.0$ (green), and $\Psi = 1.1$ (blue) in the absence of a divertor plate. The black dots shows the locations of the two current filaments. Here, $q_* = 12$ and $\zeta = 0.2$.

The red and blue curves in Fig. 2 show the safety-factor profile, $q(\Psi)$, inside and outside the magnetic separatrix, respectively. It is clear that the safety-factor generally increases with increasing Ψ. However, $q \to \infty$ as $\Psi \to 1$. In other words, the safety-factor tends to infinity as the magnetic separatrix is approached from either direction. It is apparent from the bottom panel of Fig. 2 that q approaches infinity *logarithmically* as $\Psi \to 1$ (because the plot of q versus $\log_{10}(|\Psi - 1|)$ asymptotes to a straight line as $|\Psi - 1| \to 0$). In other words, close to the separatrix, we can write

$$q(\Psi) \simeq -\alpha_- \, \ln(1 - \Psi) \tag{19}$$

for $\Psi < 1$, and

$$q(\Psi) \simeq -\alpha_+ \, \ln(\Psi - 1) \tag{20}$$

for $\Psi > 1$. Moreover, the figure implies that $\alpha_+ > \alpha_-$.

Figures 3 and 4 show the straight-field-line coordinate system inside and outside the magnetic separatrix, respectively. It can be seen that, as the magnetic separatrix is crossed, all of the contours of θ converge onto, and then diverge away from, the X-point. This singular behavior occurs because $|\hat{\nabla}\psi| \to \ell$ and $|\hat{\nabla}\theta| \to 1/[\ell \ln|\Psi - 1|]$ as the X-point is approached, where ℓ represents distance from the X-point in the X-Y plane

2.8 Significance of straight-field-line coordinates

To understand the significance of the straight-field-line coordinate system, suppose that the plasma is subject to a static (in the laboratory frame) magnetic perturbation that varies with θ and ϕ as $\exp[\mathrm{i}\,(m\,\theta - n\,\phi)]$. Here, m and n are integers. In other words, the perturbation (which is, of course, single-valued in the angular coordinates θ and ϕ) possesses m periods in the poloidal angle, and n periods in the toroidal angle. The curl of the perturbed, linearized, electron fluid equation of motion yields

$$n\,(\omega_E + \omega_{*\,e})\left[b^{\psi_p} - \frac{B_0}{R_0}\left(\frac{m}{q} - n\right)\xi^{\psi_p}\right] \simeq \frac{B_0}{R_0}\,\frac{m}{q}\,\eta_\| \, j_\phi, \tag{21}$$

where subscripts and superscripts denote covariant and contravariant components in the ψ_p, θ, ϕ coordinate system, respectively. Here, **b** is the perturbed magnetic field, $\boldsymbol{\xi}$ the Lagrangian electron fluid displacement, **j** the perturbed current density, and $\eta_\|$ the plasma parallel electrical resistivity.
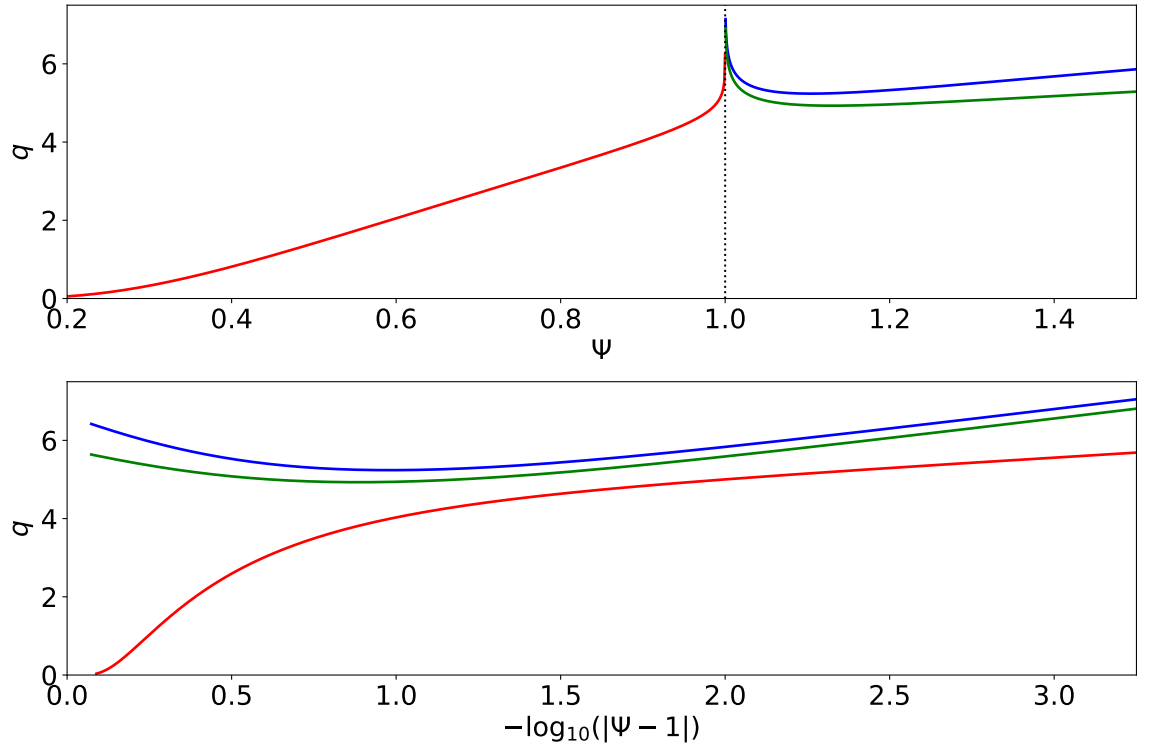
Figure 2. The safety-factor profile, $q(\Psi)$. The red curve shows the safety-factor inside the magnetic separatrix. The blue and green curves show the safety-factor outside the separatrix in the absence and in the presence of a divertor plate, respectively. Here, $q_* = 12$ and $\zeta = 0.2$.

Moreover,

$$\omega_E(\psi_p) = -\frac{d\Phi}{d\psi_p} \tag{22}$$

is the *E-cross-B frequency*, whereas

$$\omega_{*e}(\psi_p) = \frac{1}{e\,n_e}\frac{dp_e}{d\psi_p} \tag{23}$$

is the *electron diamagnetic frequency*. Here, $\Phi(\psi_p)$ is the electrostatic potential, $p_e(\psi_p)$ the electron pressure, $n_e(\psi_p)$ the electron number density, and e the magnitude of the electron charge.

Equation (21) describes how the inductive electric field generated by a time-varying magnetic field, as seen in rest frame of the local electron fluid, attempts to drive a current parallel to magnetic field-lines. On a general magnetic flux-surface, the two terms (in the large square brackets) on the left-hand side of the equation cancel one another out, and there is no driven current. In other words, the electron fluid displaces rather than allowing a parallel inductive current to flow [3]. However, it is clear from the equation that there exists a special magnetic flux-surface, termed a *rational* flux-surface, at which the safety-factor takes the rational value $q = m/n$ [12]. On the rational flux-surface, the two terms on the left-hand side of Eq. (21) cannot cancel one another out, because the second term is zero everywhere on the surface. Hence, in general, a parallel inductive current is driven on the rational flux-surface. The current is a *shielding current* that acts to suppress driven magnetic reconnection on the flux-surface [3, 16].

We can now appreciate that, by employing a straight-field-line coordinate system, we can distinguish rational magnetic flux-surfaces from irrational flux-surfaces. (A rational surface is one on which the associated safety-factor can be expressed as a rational number. Note that this definition only makes sense if the safety-factor is a flux-surface function.) We can also determine the angular variation of the particular magnetic perturbation that drives a shielding current on a particular rational surface. Finally, it is clear from that Figs. 2–4 that rational flux-surfaces exist both inside and outside the magnetic separatrix.
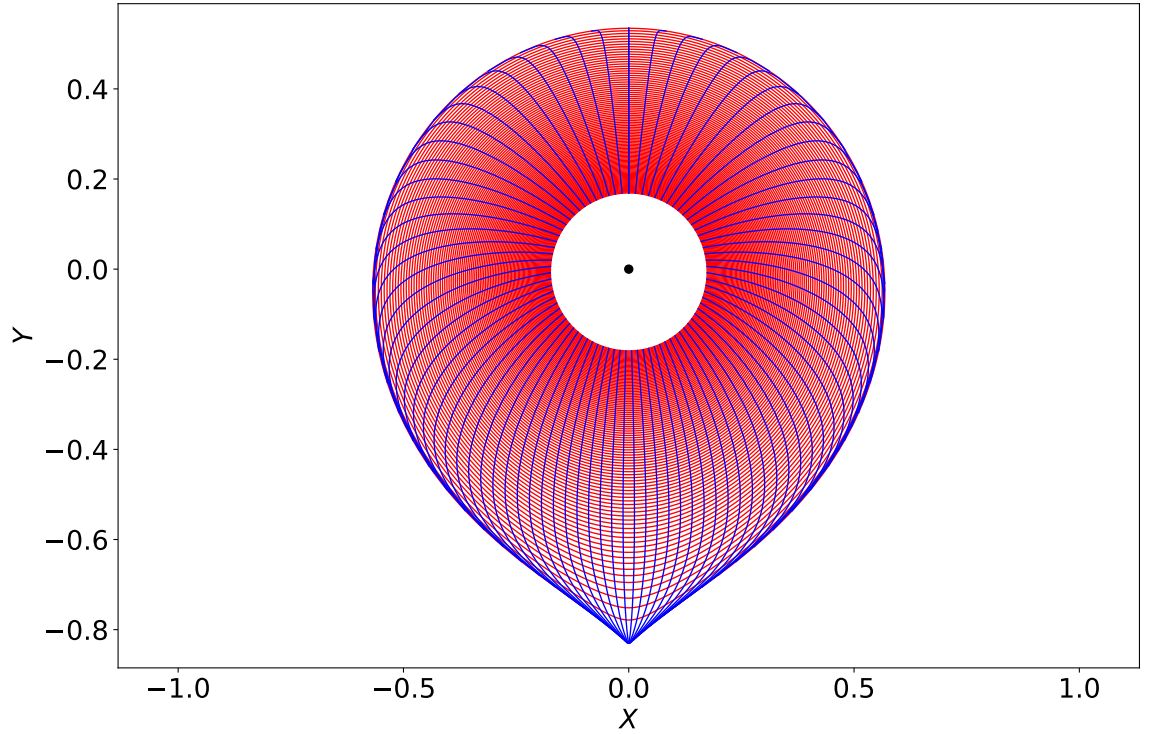
Figure 3. The straight-field-line coordinate system inside the magnetic separatrix. The red curves are surfaces of constant $\hat{\psi}$, whereas the blue curves are surfaces of constant θ. The black dot shows the location of the plasma current filament. Here, $q_* = 12$ and $\zeta = 0.2$.

2.9   Effect of divertor plate

Rational magnetic flux-surfaces exist outside the magnetic separatrix because flux-surfaces in this region form closed loops, that complete below the divertor filament, when plotted in the X-Y plane. In fact, this must be the case in an axisymmetric system otherwise the divergence of the magnetic field would be non-zero. Thus, the commonly used term "last closed magnetic flux-surface" (meaning the magnetic separatrix) is inaccurate. All of the magnetic flux-surfaces are closed. However, those outside the magnetic sepatatrix are only partially occupied by plasma because they intersect the solid divertor plate.

Suppose that the divertor plate is horizontal (i.e., parallel to the X-axis), and is situated halfway between the X-point and the divertor filament. When integrating Eqs. (13)–(16), we are really integrating along the path of a shielding current filament excited by an inductive electric field. Under normal circumstances, the filament is constrained to run parallel to magnetic field-lines. However, within the rigid divertor plate (which is assumed to be electrically conducting), the filament takes the path of least electrical resistance, which implies that it runs along the X-axis at constant ϕ. It follows that, within the divertor plate, Eqs. (13)–(16) must be replaced by

$$\frac{dX}{dL} = 1, \tag{24}$$

$$\frac{dY}{dL} = 0, \tag{25}$$

$$\frac{d\phi}{dL} = 0, \tag{26}$$

$$\frac{d\varpi}{dL} = -\frac{Y}{X^2 + Y^2}. \tag{27}$$

Again, let $q_* = 12$ and $\zeta = 0.2$. Figure 5 shows the magnetic flux-surfaces $\Psi = 0.9$, $\Psi = 1.0$, and $\Psi = 1.1$, plotted in the X-Y plane. Note that the surfaces $\Psi = 1.0$ and $\Psi = 1.1$ both have sections that run parallel to the divertor plate. Strictly speaking, these sections are not magnetic flux-surfaces (the actual magnetic flux-surfaces complete below the divertor plate, as shown in Fig. 1), but instead represent the paths of shielding current filaments.

The green curve in Fig. 2 shows the safety-factor profile calculated outside the magnetic separatrix in the presence of the divertor plate. Note that the safety-factor is decreased in the
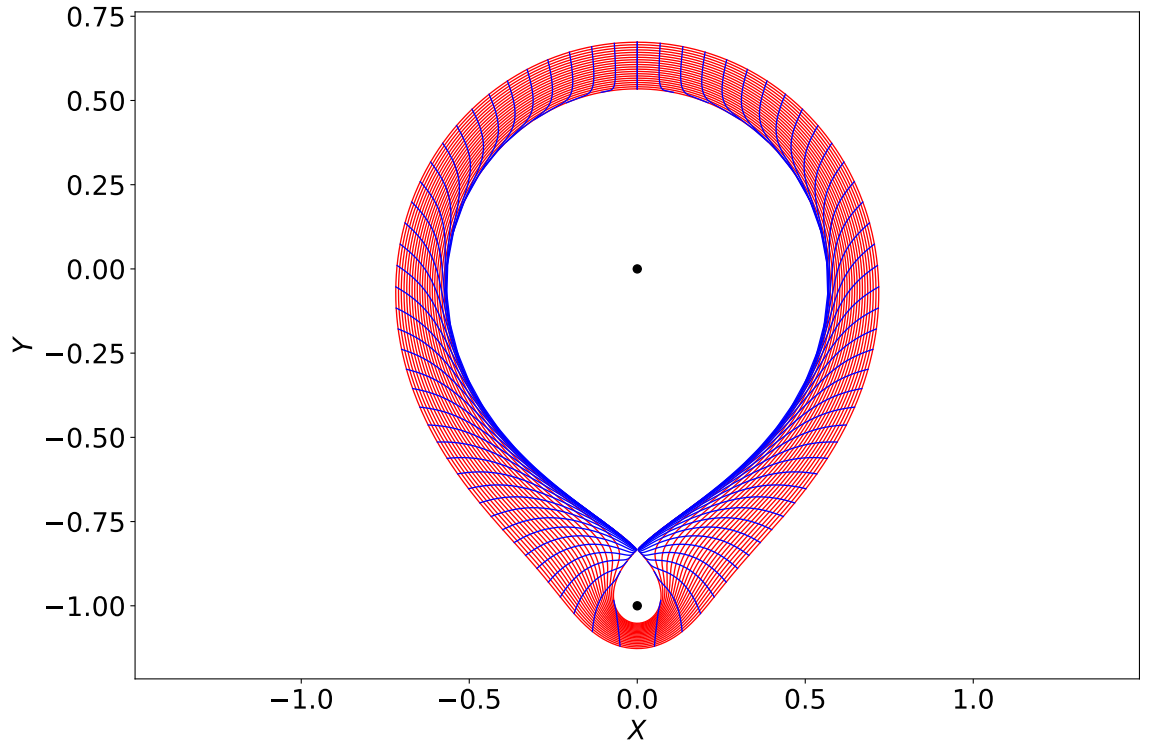
Figure 4. The straight-field-line coordinate system outside the magnetic separatrix in the absence of a divertor plate. The red curves are surfaces of constant $\hat{\psi}$, whereas the blue curves are surfaces of constant θ. The black dots shows the locations of the two current filaments. Here, $q_* = 12$ and $\zeta = 0.2$.

presence of the plate, because shielding current filaments can take a short-cuts through it, rather than having to run in loops below it.

Finally, Fig. 6 shows the straight-field-line coordinate system outside the magnetic separatrix in the presence of the divertor plate. Observe that the divertor plate is a surface of constant θ.

3   Improved model of a magnetically diverted plasma

3.1   Introduction

The model described in Sect. 2 has the unrealistic feature that $q = 0$ at the magnetic axis. This feature is an artifact of treating the plasma current as a filament, rather than a spatially extended distribution. In this section, we shall attempt to construct an improved model.

3.2   Equilibrium magnetic field

Let R, ϕ, Z be conventional cylindrical coordinates that are coaxial with the plasma torus. Thus, $\nabla R \times \nabla \phi \cdot \nabla Z = 1/R$. We can express the equilibrium magnetic field in the divergence-free manner [16]

$$\mathbf{B} = \nabla \phi \times \nabla \psi_p + B_0 \, R_0 \, g \, \nabla \phi = \nabla(\phi - q \, \theta) \times \nabla \psi_p. \tag{28}$$

Here, ϕ is a true toroidal angle, ψ_p the true poloidal magnetic flux (divided by 2π), $g(\psi_p)$ an arbitrary (dimensionless) flux-function, $q(\psi_p)$ the safety-factor, R_0 the major radius of the magnetic axis, and B_0 the vacuum toroidal magnetic field-strength on the axis (which implies that $g = 1$ in the vacuum region surrounding the plasma). The previous equation is only self-consistent if

$$\nabla \psi_p \times \nabla \theta \cdot \nabla \phi = \frac{B_0 \, R_0 \, g}{R^2 \, q}. \tag{29}$$

It is helpful to define a magnetic flux-surface label, r, with the dimensions of length, as follows [16]:

$$\frac{d\psi_p}{dr} = \frac{B_0 \, r \, g}{q}. \tag{30}$$

It is easily demonstrated that

$$\nabla r \times \nabla \theta \cdot \nabla \phi = \frac{R_0}{R^2 \, r}. \tag{31}$$
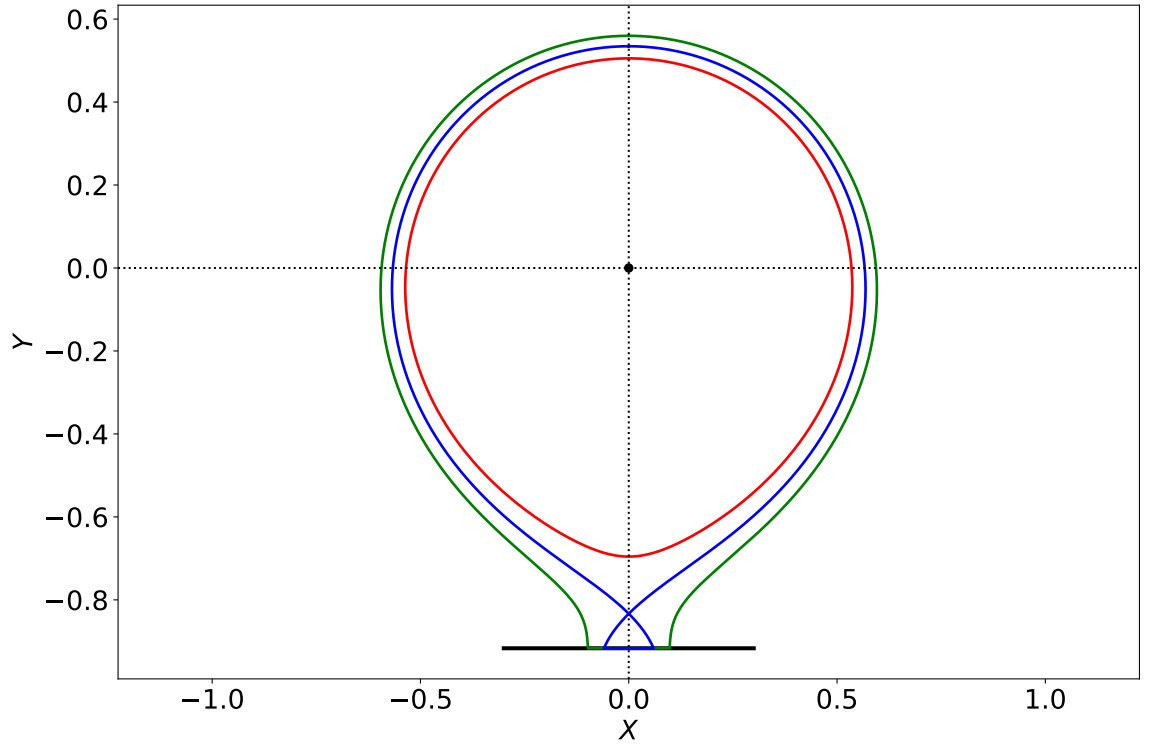
Figure 5. The magnetic flux-surfaces $\Psi = 0.9$ (red), $\Psi = 1.0$ (green), and $\Psi = 1.1$ (blue) in the presence of a divertor plate located halfway between the X-point and the divertor filament. The black dot shows the location of plasma current filament, and the horizontal black line shows the location of the divertor plate. Here, $q_* = 12$ amd $\zeta = 0.2$.

Here, r can be interpreted as the mean minor radius of a given magnetic flux-surface. Suppose that the magnetic separatrix corresponds to the flux-surface $r = a$. Thus, we can interpret a as the mean minor radius of the plasma. Moreover, flux-surfaces with $r < a$ lie inside the separatrix, whereas those with $r > a$ lie outside.

3.3   Model safety-factor profile

Let us adopt a model safety-factor profile inspired by the analysis of Sect. 2. Let $\hat{r} = r/a$. Suppose that

$$q(\hat{r}) = q_0 - \alpha_- \ln\left(1 - \hat{r}^{\,2}\right) \tag{32}$$

for $\hat{r} < 1$, and

$$q(\hat{r}) = -\alpha_+ \ln\left(\hat{r}^{\,2} - 1\right) \tag{33}$$

for $\hat{r} > 1$, where

$$\alpha_- = -\frac{q_{95} - q_0}{\ln(1 - \hat{r}_{95}^2)}, \tag{34}$$

$$\alpha_+ = -\frac{q_{105}}{\ln(\hat{r}_{105}^2 - 1)}. \tag{35}$$

Here, q_0 is the safety-factor on the magnetic axis ($\hat{r} = 0$), q_{95} is the safety-factor on the magnetic flux-surface that encloses 95% of the poloidal magnetic flux enclosed by the magnetic separatrix, $\hat{r}_{95}$ is the $\hat{r}$-coordinate of the 95% flux-surface, q_{105} is the safety-factor on the magnetic flux-surface that encloses 105% of the poloidal magnetic flux enclosed by the magnetic separatrix, and $\hat{r}_{105}$ is the $\hat{r}$-coordinate of the 105% flux-surface.

3.4   Poloidal magnetic flux

We wish to determine the poloidal flux in the vicinity of the magnetic separatrix. Let $\psi_p = B_0\, a^2\, \psi$. It follows from Eq. (30) that

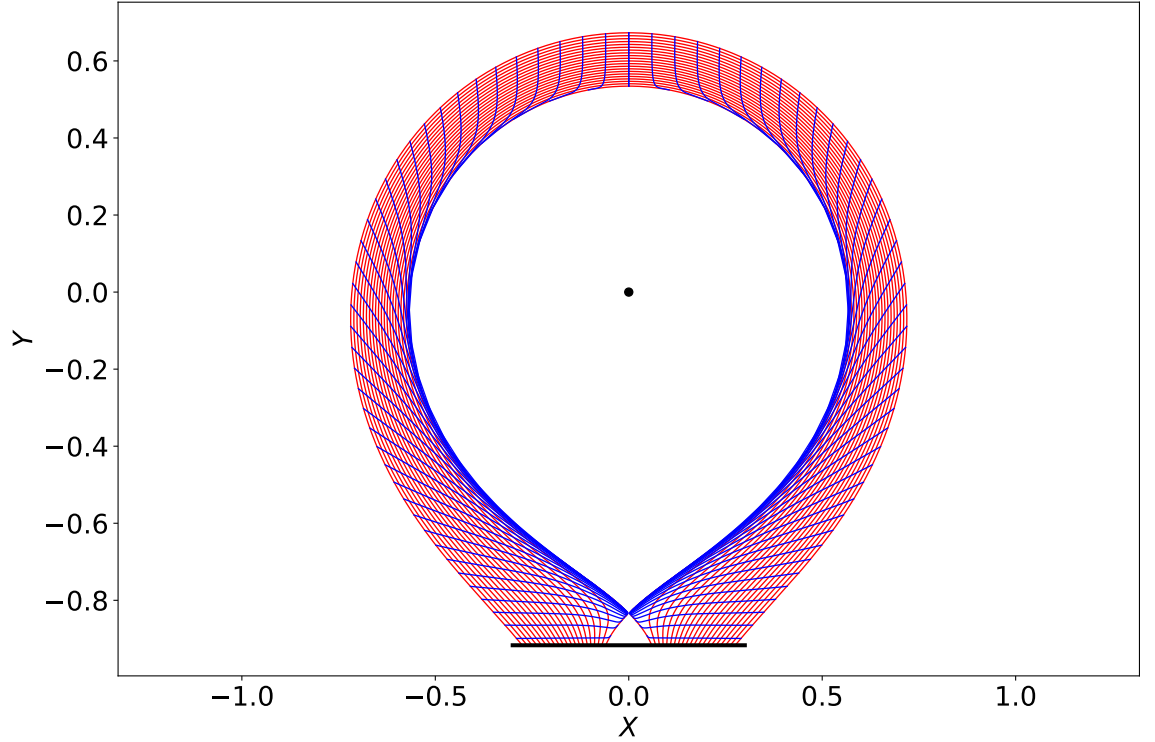$$\frac{d\psi}{d\hat{r}} \simeq \frac{\hat{r}}{q}, \tag{36}$$

Figure 6. The straight-field-line coordinate system outside the magnetic separatrix in the presence of a divertor plate located halfway between the X-point and the divertor filament. The red curves are surfaces of constant $\hat{\psi}$, whereas the blue curves are surfaces of constant θ. The black dot shows the location of the plasma filament, and the horizontal black line shows the location of the divertor plate. Here, $q_* = 12$ and $\zeta = 0.2$.

assuming that we can set $g \simeq 1$ close to the separatrix.

For $\hat{r} < 1$, Eqs. (32) and (36) yield

$$\frac{d\psi}{d\hat{r}} = \frac{\hat{r}}{q_0 - \alpha_- \, \ln(1 - \hat{r}^{\,2})}, \tag{37}$$

which can be integrated to give

$$\psi(\hat{r}) = \frac{\mathrm{e}^{\,q_0/\alpha_-}}{2\,\alpha_-} \left\{ E_1\!\left(\frac{q_0}{\alpha_-}\right) - E_1\!\left[\frac{q_0}{\alpha_-} - \ln\left(1 - \hat{r}^{\,2}\right)\right] \right\}, \tag{38}$$

where $E_1(x)$ is an exponential integral [17]. Hence,

$$\psi(1) = \frac{\mathrm{e}^{\,q_0/\alpha_-}}{2\,\alpha_-} \, E_1\!\left(\frac{q_0}{\alpha_-}\right) \tag{39}$$

is the poloidal magnetic flux (divided by $2\pi\,B_0\,a^2$) enclosed within the magnetic separatrix. Let us define the *normalized poloidal magnetic flux*, $\Psi(\hat{r}) = \psi(\hat{r})/\psi(1)$. Thus, $\Psi = 0$ on the magnetic axis, $\Psi = 1$ on the magnetic separatrix, and $\Psi > 1$ outside the separatrix. It follows that

$$\Psi(\hat{r}) = 1 - \frac{E_1[q_0/\alpha_- - \ln(1 - \hat{r}^{\,2})]}{E_1(q_0/\alpha_-)} = 1 - \frac{E_1(q/\alpha_-)}{E_1(q_0/\alpha_-)}. \tag{40}$$

By definition, $\Psi(\hat{r}_{95}) = 0.95$, so

$$\frac{E_1(q_{95}/\alpha_-)}{E_1(q_0/\alpha_-)} = 0.05. \tag{41}$$

Assuming that q_0 and q_{95} are specified, the previous equation can be solved to give α_-, which then allows $\hat{r}_{95}$ to be determined from Eq. (34).

For $\hat{r} > 1$, Eqs. (33) and (36) yield

$$\frac{d\psi}{d\hat{r}} = -\frac{\hat{r}}{\alpha_+ \ln(\hat{r}^{\,2} - 1)}, \tag{42}$$
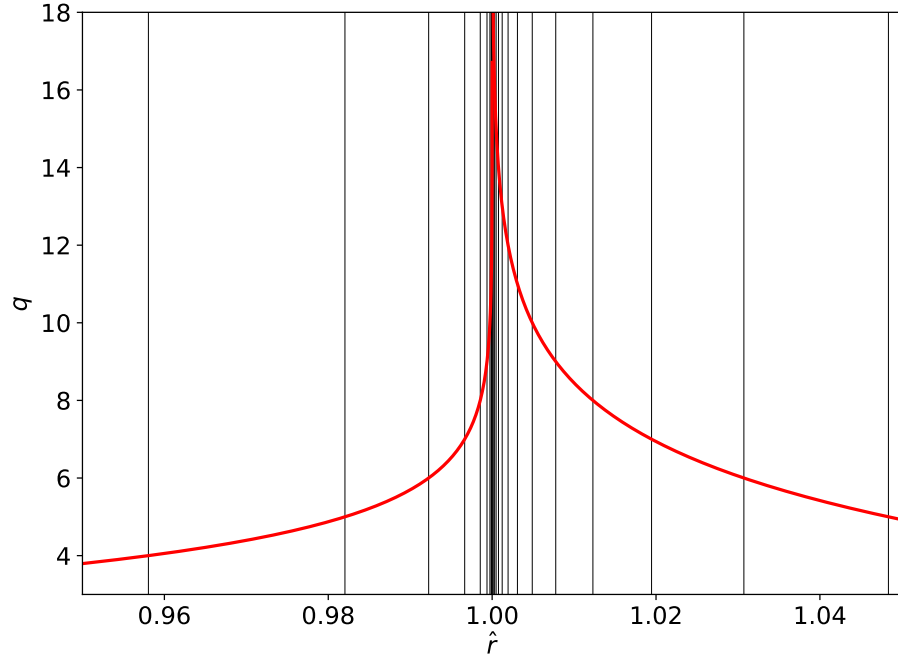
Figure 7. The model safety-factor profile in the vicinity of the magnetic separatrix, calculated for $q_0 = 1.01$, $q_{95} = 3.5$, and $q_{105} = 4.0$. The black vertical lines show the locations of the $n = 1$ rational surfaces.

which can be integrated to give

$$\psi(\hat{r}) = \psi(1) + \frac{E_1[-\ln(\hat{r}^{\,2} - 1)]}{2\,\alpha_+}. \tag{43}$$

Thus,

$$\Psi(\hat{r}) = 1 + \frac{\alpha_-}{\alpha_+}\, e^{-q_0/\alpha_-}\, \frac{E_1[-\ln(\hat{r}^{\,2} - 1)]}{E_1(q_0/\alpha_-)} = 1 + \frac{\alpha_-}{\alpha_+}\, e^{-q_0/\alpha_-}\, \frac{E_1(q/\alpha_+)}{E_1(q_0/\alpha_-)}, \tag{44}$$

where use has been made of Eq. (39). By definition, $\Psi(\hat{r}_{105}) = 1.05$. Hence, Eqs. (41) and (44) can be combined to give

$$\frac{E_1(q_{105}/\alpha_+)}{\alpha_+} = e^{\,q_0/\alpha_-}\, \frac{E_1(q_{95}/\alpha_-)}{\alpha_-}. \tag{45}$$

Assuming that q_{105} is specified, the previous equation can be solved to give α_+, which then allows $\hat{r}_{105}$ to be determined from Eq. (35).

Consider a plasma equilibrium characterized by $q_0 = 1.01$, $q_{95} = 3.5$, and $q_{105} = 4.0$. We can solve Eqs. (41) and (45) to give $\alpha_- = 1.196$ and $\alpha_+ = 2.163$. Equations (34) and (35) then reveal that $\hat{r}_{95} = 0.9355$ and $\hat{r}_{105} = 1.076$. The resulting model safety-factor profile in the vicinity of the magnetic separatrix is shown in Fig. 7.

4 Plasma response theory
4.1 Introduction
The aim of this section is analyze the response of a tokamak plasma possessing a magnetic separatrix to a static RMP of toroidal mode number n.

4.2 Ideal-MHD perturbation
Suppose that the plasma equilibrium is subject to a static magnetic perturbation that possesses n periods in the toroidal direction, and is such that [18]

$$\frac{r\, b^r(r,\theta,\phi)}{B_0\, R_0} = i\left(\frac{R_0}{R}\right)^2 \sum_m \psi_m(r)\, e^{\,i\,(m\,\theta - n\,\phi)}, \tag{46}$$

where $b^r = \mathbf{b} \cdot \nabla r$, $\mathbf{b}$ is the perturbed magnetic field, and the $\psi_m(r)$ are dimensionless functions. Note that the perturbation consists of a single toroidal harmonic, but multiple coupled poloidal harmonics characterized by the set of integer poloidal mode numbers m. Everywhere in the

plasma, apart from the immediate vicinity of the various rational surfaces, the perturbation is governed by the linearized equations of marginally-stable, ideal-magnetohydrodynamics (MHD) [20]. These equations reduce to a set of coupled ordinary differential equations (o.d.e.s) that take the form [16, 18]

$$r \frac{d\psi_m}{dr} = \sum_{m'} \frac{L_m^{m'} Z_{m'} + M_m^{m'} \psi_{m'}}{m' - n q}, \tag{47}$$

$$(m - n q) \, r \, \frac{d}{dr}\left(\frac{Z_m}{m - n q}\right) = \sum_{m'} \frac{N_m^{m'} Z_{m'} + P_m^{m'} \psi_{m'}}{m' - n q}. \tag{48}$$

Here, the (dimensionless) $Z_m(r)$ functions are related to the perturbed toroidal magnetic field. Moreover, the (dimensionless) $L_m^{m'}(r)$, $M_m^{m'}(r)$, $N_m^{m'}(r)$, and $P_m^{m'}(r)$ coefficients are determined by the equilibrium profiles and the metric elements of the r, θ, ϕ straight-field-line coordinate system [18]. Note that Eqs. (47) and (48) are singular at rational magnetic flux-surfaces at which $q = m/n$.

The locations of the $n = 1$ rational surfaces for our model safety-factor profile are indicated in Fig. 7. It can be seen that rational surfaces accumulate in the vicinity of the magnetic separatrix, where $q(\hat{r})$ has a logarithmic singularity. Moreover, rational surfaces exist both inside and outside the separatrix.

4.3   Behavior in vicinity of rational surface

Consider the solution of the ideal-MHD o.d.e.s, (47) and (48), in the vicinity of a rational surface, of radius r_s, where $q(r_s) = m/n$, and m is the resonant poloidal mode number. Let $x = r - r_s$. At small values of $|x|$, the function $\psi_m(r)$ takes the form [16, 18]

$$\psi_m(r_s + x) = A_L^{\pm} \, |x|^{\nu_L}(1 + \lambda_L \, x) + A_S^{\pm} \, \mathrm{sgn}(x) \, |x|^{\nu_S} + A_C \, x + \mathcal{O}(x^2), \tag{49}$$

where

$$\nu_L = \frac{1}{2} - \sqrt{-D_I}, \tag{50}$$

$$\nu_S = \frac{1}{2} + \sqrt{-D_I}, \tag{51}$$

$$D_I = -L_0 \, P_0 - \frac{1}{4}, \tag{52}$$

$$L_0 = -\left(\frac{L_m^m}{m \, s}\right)_{r_s}, \tag{53}$$

$$P_0 = -\left(\frac{P_m^m}{m \, s}\right)_{r_s}, \tag{54}$$

$$s = \frac{d \ln q}{d \ln r}, \tag{55}$$

and λ_L and A_C are defined in Refs. [16] and [18]. The superscripts $+$ and $-$ correspond to $x > 0$ and $x < 0$, respectively. Here, $A_L^{\pm}$ are known as the *coefficients of the large solution*, whereas $A_S^{\pm}$ are termed the *coefficients of the small solution*. The *Mercier interchange stability parameter*, D_I, is assumed to be negative. (Otherwise, the plasma in the vicinity of the rational surface would be unstable to localized ideal interchange modes [21].) Note that ν_L and ν_S are known as *Mercier indices*.

In general, the response of the plasma in the vicinity of a given rational surface to the RMP is predominately *tearing parity* in nature [19]. For the case of a tearing parity response, the coefficients of the large solution to the left and the right of a rational surface are equal to one another. In other words, $A_L^{+} = A_L^{-} = A_L$. Note, however, that the coefficients of the small solution to the left and the right of a rational surface are not, in general, equal to one another.

4.4   Plasma response equation

Let us index the various rational surfaces in the plasma by means of an integer k. Note that this is possible even if there are an infinite number of such surfaces. Thus, the kth rational surface possesses the minor radius r_k, the resonant poloidal mode number m_k, the coefficient of the large

solution $A_{L\,k}$, the coefficients of the small solution $A_{S\,k}^{\pm}$, and the Mercier indices $\nu_{L\,k}$ and $\nu_{S\,k}$. It is helpful to define the quantities [16, 18]

$$\Psi_k = r_k^{\nu_{L\,k}} \left(\frac{\nu_{S\,k} - \nu_{L\,k}}{L_{m_k}^{m_k}} \right)_{r_k}^{1/2} A_{L\,k}, \tag{56}$$

$$\Delta\Psi_k = r_k^{\nu_{S\,k}} \left(\frac{\nu_{S\,k} - \nu_{L\,k}}{L_{m_k}^{m_k}} \right)_{r_k}^{1/2} (A_{S\,k}^+ - A_{S\,k}^-). \tag{57}$$

at each rational surface. Here, the complex dimensionless parameter Ψ_k is a measure of the driven reconnected magnetic flux at the kth rational surface, whereas the complex dimensionless parameter $\Delta\Psi_k$ is a measure of the strength of the radially localized shielding current that flows around the surface.

The response of a tokamak plasma to an RMP takes the general form [16, 18]

$$\Delta\Psi_k = \sum_{k'} E_{kk'}\,\Psi_{k'} + \chi_k, \tag{58}$$

and specifies the shielding current that is excited in the vicinity of the kth rational surface in response to reconnected magnetic flux at the other rational surfaces, as well as to the RMP. Here, $E_{kk'}$ is an Hermitian matrix that can be determined entirely from the ideal-MHD o.d.e.s, (47) and (48), subject to physical boundary conditions at small and large r [16, 18]. Moreover, the real quantity E_{kk} can be interpreted as the *tearing stability index* [20] of a tearing mode that only reconnects magnetic flux at the kth rational surface. Finally, the χ_k specify the poloidal harmonics of the RMP [18, 19].

4.5 Resistive layers

In reality, the shielding current that flows in the vicinity of the kth rational surface does so in a resistive layer whose thickness (in r), δ_k, is much less than r_k [20]. We can define the complex dimensionless *layer response index*,

$$\Delta_k \equiv \frac{\Delta\Psi_k}{\Psi_k}, \tag{59}$$

which characterizes the tearing parity response of the plasma in the layer to the magnetic perturbation external to the layer. Equations (58) and (59) can be combined to give

$$\sum_{k'} (\Delta_k\,\delta_{kk'} - E_{kk'})\,\Psi_k = \chi_k, \tag{60}$$

where $\delta_{kk'}$ is a Kronecker delta symbol. The previous equation is termed the *plasma response equation*, and specifies the reconnected magnetic flux driven by the RMP at each rational surface in the plasma.

Note that the derivation of Eq. (60) depends crucially on the principle of *asymptotic matching* [20]. According to this principle, the plasma response is governed by the equations of linearized, marginally-stable, ideal-MHD throughout most of the plasma. However, these equations become singular at the various rational surfaces in the plasma. [See Eqs. (47) and (48).] The singularities are resolved by asymptotically matching the ideal-MHD solution to resistive layer solutions at each rational surface in the plasma.

4.6 Ideal and vacuum responses

Suppose, for the sake of argument, that the plasma only contains a single rational surface. In this case, the plasma response equation, (60), reduces to

$$\Psi_k = \frac{\chi_k}{\Delta_k - E_{kk}}. \tag{61}$$

Alternatively, Eq. (58) yields

$$\Delta\Psi_k = E_{kk}\,\Psi_k + \chi_k. \tag{62}$$

We can distinguish two asymptotic limits. In the first limit, $|\Delta_k| \gg |E_{kk}|$. In this limit, the shielding current excited at the rational surface is sufficiently strong that driven magnetic reconnection is largely suppressed at the surface [3, 16]. In other words, $\Psi_k \simeq 0$. We term this an *ideal response*, because it is the exactly the same response as one would get by imposing the

ideal-MHD flux-freezing constraint that the topology of the magnetic field cannot change at the rational surface: i.e., $\Psi_k = 0$ [2]. In the second limit, $|\Delta_k| \ll |E_{kk}|$. In this limit, the shielding current is too weak to prevent driven magnetic reconnection from occurring at the rational surface. Thus, $\Psi_k \simeq -\chi_k/E_{kk}$. We term this a *vacuum response*, because it is exactly the same response as one would get by imposing the vacuum constraint that no shielding current flows at the rational surface: i.e., $\Delta\Psi_k = 0$.

In a region of the plasma in which the response to the RMP lies in the ideal regime (i.e., $|\Delta_k|/|E_{kk}| \gg 1$ at all rational surfaces), the perturbed magnetic field has a strong dependence on the equilibrium magnetic field, because the equilibrium field determines the locations of the rational surfaces on which the constraints $\Psi_k \simeq 0$ have to be imposed. On the other hand, in a region of the plasma in which the response lies in the vacuum regime (i.e., $|\Delta_k|/|E_{kk}| \ll 1$ at all rational surfaces), the perturbed magnetic field has no (local) dependence on the equilibrium magnetic field. This is the case because we can write the perturbed field in a current-free region in the form $\mathbf{b} = \nabla V$, where the vacuum potential satisfies $\nabla^2 V = 0$, which completely independent of the equilibrium field. Moreover, writing the perturbed magnetic field in this form automatically satisfies the constraints that $\Delta\Psi_k = 0$ at the rational surfaces. Thus, in the vacuum regime, there is no need for us to determine the locations of the rational surfaces, which means that we do not have to employ a straight-field-line coordinate system, which implies that there is no reason for our adopted coordinate system to become singular anywhere.

5 Behavior close to magnetic separatrix

5.1 Introduction

The aim of this section is to investigate asymptotic matching in the immediate vicinity of the magnetic separatrix.

5.2 Spacing between successive rational surfaces

Suppose that $\hat{r}_{k+1} > \hat{r}_k$ for all values of k, where $\hat{r}_k = r_k/a$. In other words, suppose that the rational surfaces are indexed in order of increasing minor radius. In the vicinity of the magnetic separatrix, Eqs. (32) and (33) yield

$$\hat{r}_k \simeq \left[1 - \exp\left(-\frac{m_k}{n\,\alpha_-} \right) \right]^{1/2} \tag{63}$$

for $\hat{r}_k < 1$, and

$$\hat{r}_k = \left[1 + \exp\left(-\frac{m_k}{n\,\alpha_+} \right) \right]^{1/2} \tag{64}$$

for $\hat{r}_k > 1$.

The spacing (in $\hat{r}$) between successive rational surfaces is

$$\hat{\epsilon}_k(\hat{r}_k) = \frac{d\hat{r}_k}{dm_k} \tag{65}$$

for $\hat{r}_k < 1$, and

$$\hat{\epsilon}_k(\hat{r}_k) = -\frac{d\hat{r}_k}{dm_k} \tag{66}$$

for $\hat{r}_k > 1$. Thus,

$$\hat{\epsilon}_k(\hat{r}_k) = \frac{1 - \hat{r}_k^2}{2\,n\,\alpha_-\,\hat{r}_k} \tag{67}$$

for $\hat{r}_k < 1$, and

$$\hat{\epsilon}_k(\hat{r}_k) = \frac{\hat{r}_k^2 - 1}{2\,n\,\alpha_+\,\hat{r}_k} \tag{68}$$

for $\hat{r}_k > 1$. Note that the spacing between successive rational surfaces tends to zero linearly as the magnetic separatrix ($\hat{r}_k = 1$) is approached.

5.3 Magnetic shear

In the vicinity of the magnetic separatrix, the magnetic shear can be written

$$s(\hat{r}) \equiv \frac{\hat{r}}{q}\frac{dq}{d\hat{r}} \simeq -\frac{1}{(\hat{r} - 1)\,\ln(2\,|\hat{r} - 1|)}. \tag{69}$$

Observe that the magnitude of the shear becomes infinite as the magnetic separatrix ($\hat{r} = 1$) is approached.

5.4   Resistive layer quantities

It is helpful to define the following quantities that parameterize a general resistive layer [22]:

$$\ln \Lambda = 24 - \ln \left[\left(\frac{n_e}{10^6} \right)^{1/2} \left(\frac{e}{T_e} \right) \right], \tag{70}$$

$$\tau_{ei} = \frac{6\sqrt{2}\,\pi^{3/2}\,\epsilon_0^2\,m_e^{1/2}\,T_e^{3/2}}{Z\,\ln \Lambda\,e^4\,n_e}, \tag{71}$$

$$\eta_\parallel = \frac{m_e}{1.96\,n_e\,e^2\,\tau_{ei}}, \tag{72}$$

$$\tau_R = \frac{\mu_0\,r^2}{\eta_\parallel}, \tag{73}$$

$$\tau_A = \frac{R_0\,\sqrt{\mu_0\,m_i\,n_e}}{B_0}, \tag{74}$$

$$\tau_\perp = \frac{r^2}{\chi_\perp}, \tag{75}$$

$$\tau_\phi = \frac{r^2}{\chi_\varphi}, \tag{76}$$

$$d_\beta = \frac{\sqrt{(5/3)\,m_i\,(T_e + T_i)}}{e\,B_0}, \tag{77}$$

$$S = \frac{\tau_R}{\tau_A}. \tag{78}$$

Here, Z is the effective ion charge number, $T_e(r)$ the electron temperature, $T_i(r)$ the ion temperature, m_e the electron mass, m_i the ion mass, $\chi_\perp(r)$ the perpendicular energy diffusivity, and $\chi_\phi(r)$ the perpendicular momentum diffusivity. Furthermore, $\tau_R(r)$ is the resistive diffusion time, $\tau_A(r)$ the Alfvén time, $\tau_\perp(r)$ the energy confinement time, $\tau_\phi(r)$ the momentum confinement time, $d_\beta(r)$ the ion sound radius, and $S(r)$ the Lundquist number.

5.5   Resistive layer equation

Let $Y(r)\,\exp[\,\mathrm{i}\,(m\,\theta - n\,\phi)]$ represent the perturbed electron fluid stream-function in the laboratory frame. Consider the resistive layer centered on the kth rational surface. Let $X = S^{1/3}\,(r - r_k)/r_k$, where S is evaluated at radius r_k. We can write

$$\overline{Y}(p) = \int_{-\infty}^{\infty} Y(X)\,\mathrm{e}^{-\mathrm{i}\,p\,X}\,dX. \tag{79}$$

The boundary conditions are that $\overline{Y}(p) \to 0$ as $p \to \infty$, and

$$\overline{Y}(p) = Y_0 \left[\frac{S^{-1/3}\,\Delta_k}{\pi\,p} + 1 + \mathcal{O}(p) \right] \tag{80}$$

at small values of p [22, 23]. Here, Y_0 is an arbitrary constant, and Δ_k is the complex (dimensionless) layer response index introduced in Eq. (59).

Suppose that the resistive layer physics is controlled by the low-β, three-field, extended-MHD model described in Ref. [22]. In this case, the Fourier transformed layer equations reduce to the following equation:

$$\frac{d}{dp}\left[A(p)\,\frac{d\overline{Y}}{dp} \right] - \frac{B(p)}{C(p)}\,p^2\,\overline{Y} = 0, \tag{81}$$

where

$$A = \frac{(n\,s)^2\,p^2}{-\mathrm{i}\,(Q_E + Q_e) + p^2}, \tag{82}$$

$$B = -\mathrm{i}\,Q_E\,(Q_E + Q_i) - \mathrm{i}\,(Q_E + Q_i)\,(P_\varphi + P_\perp)\,p^2 + P_\varphi\,P_\perp\,p^4, \tag{83}$$

$$C = -\mathrm{i}\,(Q_E + Q_e) + \left[P_\perp - \mathrm{i}\,(Q_E + Q_i)\,D^2 \right] p^2 + (1 + 1/\tau)\,P_\varphi\,D^2\,p^4. \tag{84}$$

Here,

$$\tau = -\frac{\omega_{*\,e}}{\omega_{*\,i}}, \tag{85}$$

$$Q_E = S^{1/3} \, n \, \omega_E \, \tau_A, \tag{86}$$

$$Q_{e,i} = S^{1/3} \, n \, \omega_{*e,i} \, \tau_A, \tag{87}$$

$$D = S^{1/3} \left(\frac{\tau}{1+\tau} \right)^{1/2} \hat{d}_\beta, \tag{88}$$

$$P_\perp = \frac{\tau_R}{\tau_\perp}, \tag{89}$$

$$P_\phi = \frac{\tau_R}{\tau_\phi}, \tag{90}$$

and

$$\omega_{*\,i}(r) = -\frac{1}{e \, n_e} \frac{dp_i}{d\psi_p} \tag{91}$$

is the *ion diamagnetic frequency*. Moreover, $p_i(r)$ is the ion pressure, and $\hat{d}_\beta = d_\beta/r$. As before, all quantities are evaluated at radius r_k.

5.6 Solution of resistive layer equation

As we saw in Sect. 5.3, the magnetic shear becomes very large as the magnetic separatrix is approached. If we treat $(n\,s)^2$ as much larger than the other parameters (e.g., Q_E, Q_e, $P_\perp$, D) that appear in Eqs. (81)–(84) then it is clear that the first term on the left-hand side of Eq. (81) dominates the second term in the region $p \lesssim 1$. In this case, we can integrate the equation to give

$$\overline{Y}(p) = Y_0 \left\{ \frac{S^{-1/3} \, \Delta_k}{\pi} \left[\frac{1}{p} + \frac{p}{\mathrm{i}\,(Q_E + Q_e)} \right] + 1 + \mathcal{O}(p^2) \right\} \tag{92}$$

for $p \lesssim 1$, where use has been made of Eq. (80). Incidentally, the previous equation bears the hallmark of a *constant-ψ* layer response regime [20, 22].

Let $p = (n\,|s|)^{1/2} \, \hat{p}$. For $\hat{p} \gtrsim 1$, Eqs. (81)–(84) yield

$$\frac{d^2\overline{Y}}{d\hat{p}^2} - \frac{B}{C} \, \hat{p}^2 \, \overline{Y} \simeq 0, \tag{93}$$

where

$$B = -\mathrm{i}\,Q_E\,(Q_E + Q_i) - \mathrm{i}\,(Q_E + Q_i)\,(P_\varphi + P_\perp)\,(n\,|s|)\,\hat{p}^2 + P_\varphi\,P_\perp\,(n\,|s|)^2\,\hat{p}^4$$
$$\simeq P_\varphi\,P_\perp\,(n\,|s|)^2\,\hat{p}^4, \tag{94}$$

$$C = -\mathrm{i}\,(Q_E + Q_e) + \left[P_\perp - \mathrm{i}\,(Q_E + Q_i)\,D^2 \right]\,(n\,|s|)\,\hat{p}^2 + (1 + 1/\tau)\,P_\varphi\,D^2\,(n\,|s|)^2\,\hat{p}^4$$
$$\simeq (1 + 1/\tau)\,P_\varphi\,D^2\,(n\,|s|)^2\,\hat{p}^4, \tag{95}$$

which reduces to

$$\frac{d^2\overline{Y}}{dp^2} - G\,p^2\,\overline{Y} \simeq 0, \tag{96}$$

where

$$G = \frac{P_\perp}{(1 + 1/\tau)\,D^2\,n^2\,|s|^2} = \frac{\tau_A^{2/3}\,\tau_R^{1/3}}{\tau_\perp\,\hat{d}_\beta^2\,(n\,|s|)^2}. \tag{97}$$

In the language of Ref. [22], we have found a constant-ψ layer solution characterized by $\nu = 1/4$. It follows from the analysis of Ref. [22] that

$$S^{-1/3}\,\Delta_k = \frac{\nu^{\,2\nu-1}\,\pi\,\Gamma(1-\nu)}{\Gamma(\nu)}\,\left[-\mathrm{i}\,(Q_E + Q_e) \right]\,G^\nu, \tag{98}$$

where $\Gamma(z)$ is a gamma function [24]. Hence, in the continuum limit in which the resistive layers are very closely spaced,

$$\Delta_k(\hat{r}) = -\mathrm{i}\,\frac{2\pi\,\Gamma(3/4)}{\Gamma(1/4)}\,\frac{n\,(\omega_E + \omega_{*e})\,\tau_A^{1/2}\,\tau_R^{3/4}}{\tau_\perp^{1/4}\,\hat{d}_\beta^{1/2}\,(n\,|s|)^{1/2}}, \tag{99}$$

where all terms on the right-hand side are evaluated at the normalized radius $\hat{r}$. Thus, we deduce that the strong magnetic shear in the vicinity of the magnetic separatrix forces all of the resonant layers in this region to lie in the so-called *diffusive-resistive* regime introduced in Ref. [22].
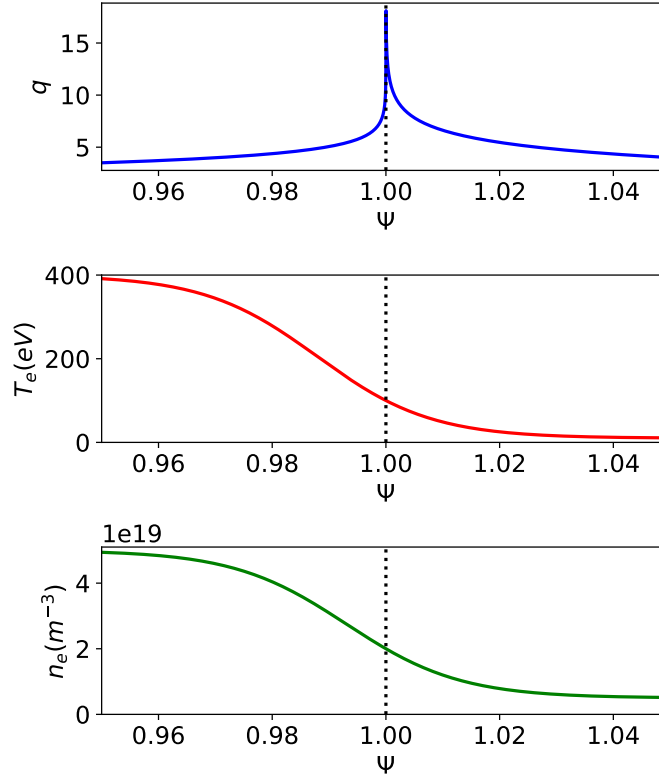
Figure 8. Model safety-factor, electron temperature, and electron number density profiles at the edge of a typical JET H-mode plasma. The vertical dotted lines show the location of the magnetic separatrix.

Finally, the thickness of a given resistive layer in p-space is $|G|^{-\nu}$ [22], so the thickness in $\hat{r}$-space is

$$\hat{\delta}_k(\hat{r}) = \frac{\tau_A^{1/2}}{\tau_R^{1/4}\,\tau_\perp^{1/4}\,\hat{d}_\beta^{1/2}\,(n\,|s|)^{1/2}}. \tag{100}$$

5.7   Mercier indices

The resistive layer solutions discussed in Sects. 5.5 and 5.6 are premised on the assumption that the Mercier indices at the rational surfaces, $\nu_{L\,k}$ and $\nu_{S\,k}$, take the respective values 0 and 1. As is described in Ref. [25], if this is not the case then the mismatch between the Mercier indices in the layer and those in the outer region (i.e., the region of the plasma that is governed by ideal-MHD) can be reconciled by matching the layer to the outer solution by means of an intermediate layer. However, the cylindrical expression for the Mercier interchange stability parameter takes the form

$$D_{I\,k} = -\frac{\mu_0}{B_0^2}\left[\frac{2\,(1-q^2)}{s^2}\,\hat{r}\,\frac{dp}{d\hat{r}}\right] - \frac{1}{4}, \tag{101}$$

where $p(\hat{r})$ is the total plasma pressure, and all quantities are evaluated at the rational surface [26]. Although the magnetic separatrix, $\hat{r}=1$, is not well-described by the cylindrical approximation, if we use the previous expression to roughly gauge how $D_{I\,k}$ varies in the vicinity of the separatrix then the fact that $q \sim \ln|\hat{r}-1|$, whereas $|s| \sim 1/(|\hat{r}-1|\,\ln|\hat{r}-1|)$ [see Eqs. (33) and (69)], indicates that the strong magnetic shear in the vicinity of the separaratrix ensures that $D_{I\,k} \to -1/4$. In this case, $\nu_{L\,k} \to 0$ and $\nu_{S\,k} \to 1$ [see Eqs. (50) and (51)], and there is no need for an intermediate layer.

5.8   Plasma parameters

Suppose that the safety-factor profile is characterized by $q_0 = 1.01$, $q_{95} = 3.5$, and $q_{105} = 4.0$, as was previously assumed.

We shall adopt the model edge electron temperature and number density profiles shown in Fig. 8. These are modified hyperbolic tangent (mtanh) profiles deduced from Figs. 1 and 2 of Ref. [27], and represent a typical reactor-relevant high-density/low-temperature pedestal in a JET H-mode plasma (discharge 84600). We shall assume that $T_i = T_e$, for the sake of simplicity.
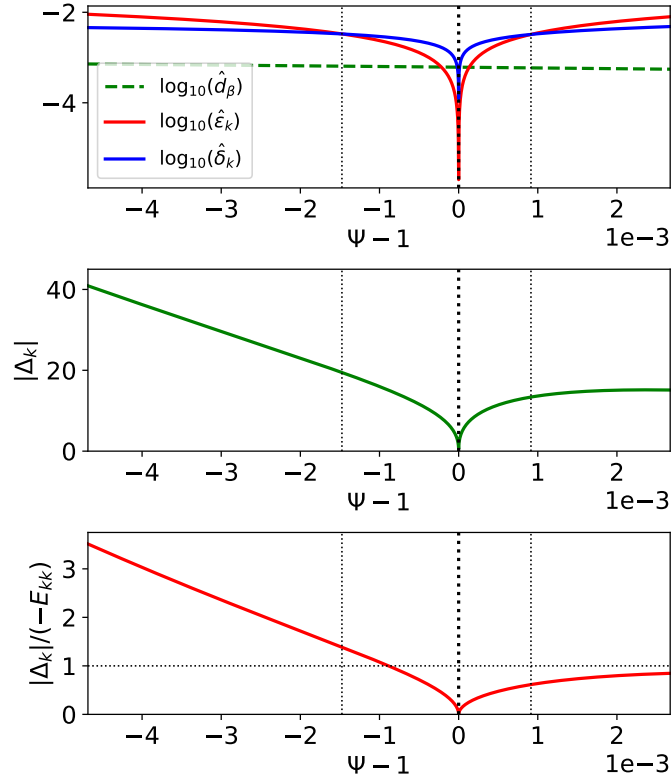
Figure 9. Overlap criterion for the resistive layers associated with an $n = 1$ RMP close to the magnetic separatrix of the JET plasma shown in Fig. 8. The bold vertical dotted lines show the location of the magnetic separatrix, whereas the faint vertical dotted lines indicate the boundaries of the region of resistive layer overlap.

Let us suppose that $\omega_E + \omega_{*e} \simeq \omega_{*e}$ close to the magnetic separatrix. This is a reasonable assumption because we have no reason to imagine that the magnitude of ω_E greatly exceeds that of ω_{*e} in the pedestal region of an H-mode tokamak plasma. In fact, Fig. 3 of Ref. [29] suggests that the magnitude of ω_E is about a factor of 5 times smaller than that of ω_{*e} in the pedestal of a typical DIII-D H-mode plasma (discharge 158115).

We can complete our model by adopting the following JET-like values of the remaining unspecified plasma parameters: $B_0 = 3.45\,\text{T}$, $R_0 = 2.96\,\text{m}$, $a = 1.25\,\text{m}$, $Z = 10.0$, $M = 2.0$, $\chi_\perp = \chi_\phi = 1\,\text{m}^2/\text{s}$ [28]. Here, M is the ion mass number, and the rather large value of Z is meant to account for the presence of a significant fraction of trapped particles, in addition to plasma impurities, close to the plasma boundary.

5.9 Overlap of resistive layers

The top panel of Fig. 9 shows the spacing (in $\hat{r}$) between successive rational surfaces $\hat{\epsilon}_k(\Psi)$, as well as the resistive layer width (in $\hat{r}$), $\hat{\delta}_k(\Psi)$, calculated in the vicinity of the magnetic separatrix for the case of an $n = 1$ RMP applied to our model JET equilibrium. It can be seen that the spacing between rational surfaces and the resistive layer width both tend to zero as the separatrix ($\Psi = 1$) is approached. However, the rational surface spacing tends to zero faster than the layer width. Consequently, the resistive layers overlap one another in the immediate vicinity of the separatrix. In fact, the region of overlap extends from $\Psi = 0.9985$ to 1.0009. Note, from the figure, that the resistive layers overlap well before either the spacing between successive rational surfaces or the layer thickness fall below the ion gyroradius (which is approximately equal to d_β).

The middle panel of Fig. 9 shows the magnitude of the layer response index, $|\Delta_k|$. It can be seen that this quantity is zero at the separatrix, but increases steeply as we move from the separatrix into the interior of the plasma, indicating that strong shielding currents are excited in the plasma interior. The steep increase is mostly due to the fact that the magnetic shear exhibits a steep decrease as we move away from the separatrix. On the other hand, the magnitude of the layer response index seems to asymptote to a constant value as we move from the separatrix into the scape-off layer (SOL) (i.e., the region $\Psi > 1$), indicating that only comparatively weak shielding currents are excited in the SOL. The magnitude of the index fails to exhibit a steep increase as we
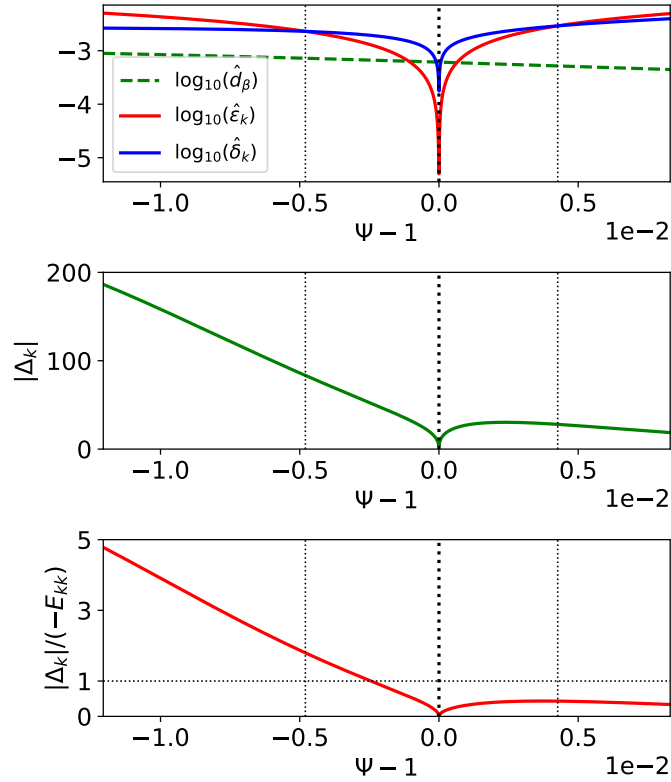
Figure 10. Overlap criterion for the resistive layers associated with an $n = 4$ RMP close to the magnetic separatrix of the JET plasma shown in Fig. 8. The bold vertical dotted lines show the location of the magnetic separatrix, whereas the faint vertical dotted lines indicate the boundaries of the region of resistive layer overlap.

move into the SOL, despite the fact that the magnetic shear is strongly decreasing, because the electron temperature falls off rapidly with increasing distance from the separatrix. In reality, the value of $|\Delta_k|$ in the SOL is probably an overestimate, because we have not taken into account the fact that shielding current filaments in the SOL run partially through the divertor plate, which is likely to increase the effective resistivity of rational magnetic flux-surfaces in this region.

The lower panel of Fig. 9 shows the ratio $|\Delta_k|/(-E_{kk})$. Here, we have used the cylindrical result $E_{kk} = -2\,|m|$ to estimate E_{kk}. It is clear that $|\Delta_k|/(-E_{kk}) \gg 1$ in the interior of the plasma. In other words, the plasma interior exhibits an ideal response to the RMP. However, $|\Delta_k|/(-E_{kk}) \lesssim 1$ in the overlap region and the SOL. In other words, it would not be unreasonable to characterize the response of the plasma in the overlap region and the SOL as being vacuum-like. Note that it is not a coincidence that the inner boundary of the overlap region corresponds approximately to the point where $|\Delta_k|/(-E_{kk}) = 1$. The plasma at the separatrix is sufficiently hot, with a typical electron temperature of $100\,\mathrm{eV}$, that $|\Delta_k|/(-E_{kk})$ would greatly exceed unity were $|s| \sim \mathcal{O}(1)$. The same factor that causes the overlap of resistive layers also causes $|\Delta_k|/(-E_{kk})$ to dip below unity very close to the separatrix, and this factor is, of course, the very strong magnetic shear in the immediate vicinity of the separatrix.

Figure 10 shows analogous data to that displayed in Fig. 9 for the case of an $n = 4$ RMP. In this case, the region of resistive layer overlap extends from $\Psi = 0.9952$ to 1.0043. Thus, the width in Ψ of the overlap region exhibits a roughly linearly scaling with n. As before, the response of the plasma interior is ideal, whereas that of the overlap region and the SOL could reasonably be characterized as being vacuum-like,

5.10 Discussion

We have seen that rational surfaces accumulate in the vicinity of the magnetic separatrix. Moreover, the resistive layers, centered on the various rational surfaces, merge into one another in a very narrow region that straddles the separatrix. Furthermore, while the plasma response in the plasma interior lies in the ideal regime, that in the region of resistive layer overlap and the SOL can reasonably be modeled as being vacuum-like. It follows that the magnetic perturbation in the plasma interior is governed by Eqs. (47) and (48). In order to solve these equations, we need to know the locations of all of the rational magnetic flux-surfaces in this region, which implies that we

must adopt a straight-field-line coordinate system. On the other hand, in the overlap region and the SOL, we can write $\mathbf{b} = \nabla V$, where $\nabla^2 V = 0$, which automatically ensures that the response is vacuum-like. In this case, there is no need to know the locations of the rational surfaces, which implies that it is not necessary to adopt a straight-field-line coordinate system.

We are now in a position to formulate a practical, yet physically justified, approach to calculating the response of a magnetically diverted tokamak plasma to an RMP. Let the inner boundary of the region of resistive layer overlap that straddles the magnetic separatrix lie at $\Psi = \Psi_c$. Note that $\Psi_c < 1$. We must solve Eqs. (47) and (48) in the region $0 < \Psi < \Psi_c$, using the straight-field-line coordinate system specified in Eq. (31), and treating the region $\Psi > \Psi_c$ as a vacuum. Of course, this is the approach taken in existing plasma response codes such as GPEC [6, 8, 10, 11], in which Ψ_c is given a value, lying just below unity, that is determined via an empirical guideline. (This course of action is adopted because GPEC cannot deal with the singularity of the straight-field-line coordinate system at $\Psi = 1$, and is taken in the hope that the neglect of a very narrow strip of plasma lying just inside the separatrix, as well as the plasma in the SOL, does not unduly affect the results of the calculation.) However, the analysis of this paper allows us to determine the correct value of Ψ_c from the edge plasma parameters, and also justifies the neglect of the plasma in the region $\Psi > \Psi_c$. The fact that the region $\Psi > \Psi_c$ is treated as a vacuum means that rational surfaces in this region do not contribute to the plasma response. In other words, the plasma response calculation only needs to take a finite, rather than an infinite, number of rational surfaces into account. Indeed, for an $n = 1$ RMP, applied to our model JET equilibrium, we only need to include rational surfaces whose resonant poloidal mode numbers are less than 8. On the other hand, for an $n = 4$ RMP, we need to include all rational surfaces whose resonant poloidal mode numbers are less than 24. Because the straight-field-line coordinate system is only required in the region $0 < \Psi < \Psi_c$, where $\Psi_c < 1$, the fact that the system becomes singular at $\Psi = 1$ is irrelevant. Indeed, we are free to choose a convenient non-singular coordinate system in the vacuum region, $\Psi > \Psi_c$.

If we suppose that q_{95} is gradually increased then, at some stage, a new rational surface will enter the domain of solution, $0 < \Psi < \Psi_c$, from the region of resistive layer overlap. Suppose that the new surface is the kth surface. The entry of the surface into the domain of solution will not cause the sudden imposition of the additional ideal constraint $\Psi_k = 0$, which would also cause a sudden change in the plasma response to the RMP, because $|\Delta_k|/|E_{kk}|$ is initially quite small, due to the large magnetic shear at $\Psi = \Psi_c$. However, as q_{95} is further increased, the new surface will move into the plasma interior, where the shear is moderate, and the ideal constraint $\Psi_k = 0$ will eventually hold. In other words, ideal constraint $\Psi_k = 0$ develops gradually, as the new surface moves into the plasma interior, rather than being imposed immediately, as soon as the surface enters the domain of solution.

6   Summary

In Sect. 2, we construct a simple model of a magnetically diverted tokamak plasma. We argue that the commonly used term "last closed magnetic flux-surface" (LCFS) is misleading. In fact, all equilibrium magnetic flux-surfaces are closed. However, flux-surfaces that lie outside the magnetic separatrix (i.e., the flux-surface that contains the X-point) are only partially occupied by plasma. We show that it is possible to calculate unique values of the safety-factor on flux-surfaces that lie both inside and outside the magnetic separatrix. We conclude that rational magnetic flux-surfaces exist in both regions. The safety-factor is shown to diverge logarithmically as the magnetic separatrix is approached.

A more realistic model of a magnetically diverted tokamak plasma is introduced in Sect. 3.

In Sect. 4, we show that the response of a magnetically diverted tokamak plasma to an externally generated, static, RMP can be formulated as an asymptotic matching problem. The response throughout most of the plasma is governed by the equations of linearized, marginally-stable, ideal-MHD. However, these equations are singular at the various rational surfaces in the plasma. The singularities are resolved by asymptotically matching the ideal-MHD solution to resistive layer solutions centered on the rational surfaces. The fact that the safety-factor diverges logarithmically as the magnetic separatrix is approached means that, in principle, the asymptotic matching problem involves an infinite number of coupled rational surfaces, the majority of which are located very close to the magnetic separatrix.

In Sect. 5, we examine the asymptotic matching problem close to the magnetic separatrix. We find that, due to the strong magnetic shear in the vicinity of the separatrix, both the spacing between successive rational surfaces and the resistive layer thickness tend to zero as the separatrix is approached. However, the rational surface spacing tends to zero faster. Consequently, there exits

a radially thin region, that straddles the magnetic separatrix, in which the resistive layers overlap. When we calculate the response to the RMP of the resistive layers in the overlap region, as well as those in the SOL, we find that the shielding currents excited in the layers are comparatively feeble, which implies that the plasma response to the RMP in these regions is essentially vacuum-like. On the other hand, the shielding currents excited in resistive layers that lie in the interior of the plasma are comparatively strong, which implies that the plasma response to the RMP in this region is essentially ideal. We are thus able to formulate a practical, yet physically justified, approach to calculating the response of a magnetically diverted tokamak plasma to an RMP. Essentially, we treat the region of the plasma that lies outside the inner boundary of the overlap region, which lies at $\Psi = \Psi_c$, where $\Psi_c < 1$, as a vacuum. This means that that rational surfaces that lie in the region $\Psi > \Psi_c$ do not contribute to the plasma response. Hence, a plasma response calculation only needs to take a finite number of rational surfaces into account. Our analysis enables us to determine Ψ_c from the edge plasma parameters. We find that $\Psi_c = 0.9985$ for an $n = 1$ RMP, and $\Psi_c = 0.9952$ for an $n = 4$ RMP, in a typical JET H-mode plasma.

Data availability

The digital data used in the figures in this paper can be obtained from the author upon reasonable request.

References

[1] J.A. Wesson, *Tokamaks*, 4th ed., (Oxford University Press, Oxford UK, 2011).

[2] A.H. Boozer, Rev. Mod. Phys. **76**, 1071 (2004).

[3] R. Fitzpatrick, Nucl. Fusion **33**, 1049 (1993).

[4] N. Pomphrey and A. Reiman, Phys. Fluids B **4**, 938 (1992).

[5] Y.Q. Liu, A. Bondeson, C.M. Fransson, B. Lennartson and C. Breitzholtz, Phys. Plasmas **7**, 3681 (2000).

[6] J.-K. Park, A.H. Boozer and A.H. Glasser, Phys. Plasmas **14**, 052110 (2007).

[7] A.H. Glasser, Phys. Plasmas **23**, 072505 (2016).

[8] J.-K. Park and N.C. Logan, Phys. Plasmas **24**, 032505 (2017).

[9] R. Fitzpatrick, Phys. Plasmas **27**, 102511 (2020).

[10] Q.M. Hu, J.-K. Park, N.C. Logan, S.M. Yang, B.A. Grierson, R. Nazikian and Q. Yu, Nucl. Fusion **61**, 106006 (2021).

[11] S. Benjamin, N.C. Logan and C. Hansen, Plasma Phys. Control. Fusion **67**, 065019 (2025).

[12] R.D. Hazeltine and J.D. Meiss, Phys. Reports **121**, 1 (1984).

[13] S. Hamada, Nucl. Fusion **2**, 23 (1962).

[14] A.H. Boozer, Phys. Fluids **24**, 1999 (1981).

[15] J.L. Johnson and R.C. Grimm, Phys. Fluids **17**, 337 (1974).

[16] R. Fitzpatrick, R.J. Hastie, T.J. Martin and C.M. Roach, Nucl. Fusion **33**, 1533 (1993).

[17] M. Abramowitz and I.A. Stegun, *Handbook of Mathematical Functions*, (Dover, New York NY, 1964), chap. 5.

[18] R. Fitzpatrick, Phys. Plasmas **31**, 102507 (2024).

[19] R. Fitzpatrick, Phys. Plasmas **24**, 072506 (2017).

[20] H.P. Furth, J. Killeen and M.N. Rosenbluth, Phys. Fluids **6**, 459 (1963).

[21] C. Mercier, Nucl. Fusion **1**, 47 (1960).

[22] R. Fitzpatrick, Phys. Plasmas **29**, 032507 (2022).

[23] A. Cole and R. Fitzpatrick, Phys. Plasmas **13**, 032503 (2006).

[24] M. Abramowitz and I.A. Stegun, *Handbook of Mathematical Functions*, (Dover, New York NY, 1964), chap. 6.

[25] R. Fitzpatrick, Phys. Plasmas **32**, 062509 (2025).

[26] A.H. Glasser, J.M. Greene and J.L. Johnson, Phys. Fluids **19**, 567 (1976).

[27] L. Frassinetti, S. Saarelma, G. Verdoolaege, M. Groth, J.C. Hillesheim, P. Bilkova, P. Bohm, M. Dunne, R. Fridström, E. Giovannozzi, et al., Nucl. Fusion **61**, 016001 (2021).

[28] Z.S. Hartwig and Y.A. Podpaly, *Magnetic Fusion Energy Formulary*, (Massachusetts Institute of Technology, Cambridge MA, 2011).

[29] R. Nazikian, C. Paz-Solden, J.D. Callen, J.S. de Grassie, D. Eldon, T.E. Evans, N.M. Ferraro, B.A. Grierson, R.J. Groebner, S.R. Haskey, et al., Phys. Rev. Lett. **114**, 105002 (2015).